TiC crystallite formation and the role of interfacial energies on the composition during the deposition process of TiC/a:C thin films

Nikolett Oláh, Zsolt Fogarassy, Attila Sulyok, Miklós Veres, George Kaptay, Katalin Balázsi

PII: S0257-8972(16)30539-4
DOI: doi: 10.1016/j.surfcoat.2016.06.047
Reference: SCT 21290

To appear in: *Surface & Coatings Technology*

Received date: 14 April 2016
Revised date: 16 June 2016
Accepted date: 17 June 2016

Please cite this article as: Nikolett Oláh, Zsolt Fogarassy, Attila Sulyok, Miklós Veres, George Kaptay, Katalin Balázsi, TiC crystallite formation and the role of interfacial energies on the composition during the deposition process of TiC/a:C thin films, *Surface & Coatings Technology* (2016), doi: 10.1016/j.surfcoat.2016.06.047

TiC crystallite formation and the role of interfacial energies on the composition during the deposition process of TiC/a:C thin films

Nikolett Oláh[1], Zsolt Fogarassy[1], Attila Sulyok[1], Miklós Veres[2], George Kaptay[3,4], Katalin Balázsi[1]

[1] *Thin Film Physics Department, Institute for Technical Physics and Materials Science, Centre for Energy Research, Hungarian Academy of Sciences (HAS), Konkoly-Thege M. str. 29-33, 1121 Budapest, Hungary,*

[2] *Institute for Solid State Physics and Optics, Wigner Research Centre for Physics, HAS, Konkoly-Thege M. str. 29-33, 1121 Budapest, Hungary*

[3] *Bay Zoltán Nonprofit Ltd for Applied Research, Engineering Division, Iglói str. 2, 3519 Miskolc, Hungary*

[4] *University of Miskolc, Department of Nanotechnology, Egyetemvaros, Miskolc, Hungary 3515*

Abstract

TiC / amorphous carbon (TiC/a:C) nanocomposite thin films were deposited from two targets by direct current (DC) magnetron sputtering system at room temperaure. The film´s composition and morphology were studied in detail by High Resolution Transmission Electron Microscopy (HRTEM), Selected Area Electron Diffraction (SAED), X-ray Photoelectron Spectroscopy (XPS) and Raman Spectroscopy. The sputtering power of carbon target (P_C) was kept at the constant 150 W, while the sputtering power of titanium target (P_{Ti}) was changed between 5 W and 150 W. Additionally, a C/Ti multilayer was deposited and characterized for comparison. The growth mechanism was derived from the XPS, Raman and HRTEM observations on the grown layer structures and it was completed by a semi-empirical equation for the dependence on the average atomic fraction of Ti. The HRTEM investigations

confirmed that the first nucleating phase is amorphous carbon due to its lowest surface energy among the possible phases. The second nucleating phase within the amorphous carbon matrix is TiC; its growth is kinetically not limited. The increase of Ti content resulted in larger TiC nanocrystallites and thinner amorphous carbon spacing between the TiC phases shown by HRTEM analysis. The characteristic texture of the crystallite structure was observed in the case of 120 W and 150 W of P_{Ti}. All observation confirmed the two main phases; amorphous carbon + carbide phase. The hcp titanium phase was not formed due to nucleation barrier. The average sputtered composition differs from the average deposited composition due to different nucleation barriers of different phases.

Keywords: TiC/a:C, growing mechanism, HRTEM, interfacial energies, nano-thermodynamics, nanocomposites

1. Introduction

Previous work revealed that C-Ti nanocomposite thin films have versatile structural and mechanical properties depending on the preparation conditions [1]. Nanocomposite coatings consisting of hard crystalline and soft amorphous nanophase have recently attracted increasing interest concerning both fundamental research and industry. The different transition metal carbides, such as titanium carbide (TiC), are relatively inexpensive and possess good mechanical properties such as high hardness, elastic modulus and low friction [2]. Therefore, TiC is extensively used as a reinforcing phase in metal matrix composites (MMC's) [3,4]. TiC is one of the most widely used hard coating materials, a suitable candidate for Ohmic contacts in microelectronic devices, used as anode in lead-acid batteries and super capacitors, an alternate to platinum as a catalyst and diffusion barrier in semiconductor technology [2]. It has been also used in phosphoric acid fuel cells (PAFCs), proton exchange membrane fuel cells (PEMFCs), water and hydrogen chloride as well as TiC

is electrochemically stable in a proton exchange membrane electrolyser [5,6]. TiC ceramics have been widely used in cutting tools, machining materials and nuclear power industry as a second dispersive phase to improve the intrinsic conductivity of the matrix and the mechanical properties such as fracture toughness of SiC ceramics/bioceramics [7,8,9].

Over the last few years, TiC/a:C nanocomposite protective surface coatings, consisting of hard TiC nanoparticles embedded in a soft amorphous matrix, have attracted a special attention because of their passivation effect on different implant materials [10,11]. The physical vapor deposition (PVD) techniques such as DC magnetron sputtering are useful to control the coating properties (density, mechanical characteristics) because these properties depend on the microstructure such as grain morphology, textures and porosity [12,13]. *Martínez et al*. [14] studied the concentration of the amorphous carbon (a:C) phase in the films, determining it by assuming that the Ti atoms are bounded to some part of the C atoms forming TiC and the remaining C atoms are present as amorphous carbon. However, TiC_X has a wide stoichiometry from x = 0.47 to 0.98 and since PVD is a non-equilibrium process, the α-Ti lattice may accept more carbon atoms due to hindered mobility of the deposited particles [15].

The main goal of our research work is the understanding of deposited TiC/a:C growth mechanism and the determination of TiC crystal formation at different Ti:C ratios. A secondary aim was to find a connection between the technological parameters (sputtering powers of C and Ti), composition and morphology of the films.

2. Material and methods

The detailed preparation steps of the TiC/a:C films were described in our previous work [16]. In the current study, 18 different coatings were examined depending on the increasing titanium target power (5 - 150 W) at fixed carbon target power (150 W). The films were sputtered simultaneously from two sources, a carbon target (99.999 %) and a titanium

target (99.995 %) by DC magnetron sputtering. Both 2" targets originate from Kurt and Lesker Co. The growth of the films was carried out at room temperature, in argon atmosphere (2.5×10^{-3} mbar) during 25 - 30 min. The applied parameters of power (P), voltage (U) and amperage (I) of the two different target (Ti and C) depending on the various sputtering times are shown in *Tab. 1*. Their thickness was found to vary between ~ 90 and ~ 330 nm depending on the sputtering power of the titanium target. For easier mechanical preparation of the samples for Transmission Electron Microscopic (TEM) analysis, thin films were deposited onto roughly the same size of oxidized Si (001) substrates having 300 nm thick oxide layer on the top. The substrates were rotated with 20 rpm during the sputtering process.

Additionally, a C/Ti/C/Ti/C/Ti multilayer was deposited for calibration purposes on the same substrate using 100 W power for each layer during 5/5/10/10/15/15 minutes. Also, additional experiments were run at 150 W of carbon power during 10.100 s of sputtering time and at 100 W of titanium power during 3.000 s of sputtering time. The analysis of C and Ti layers was separately carried out by Atomic Force Microscope (AFM) and Transmission Electron Microscope (TEM). The density values have been calculated from weight measurement combined with thickness measuremenet using AFM and TEM. The thickness was measured in a large number of cross sections, and the average value was used for density calculation.

P_{Ti} (W)	U_{Ti} (V)	I_{Ti} (A)	P_C (W)	U_C (V)	I_C (A)	t (min)
5	369	0.02	150	640	0.24	30
10	306	0.04	150	635	0.24	30
15	315	0.06	150	633	0.24	30
20	328	0.07	150	631	0.24	30
25	336	0.08	150	630	0.25	30
30	346	0.10	150	629	0.25	30
35	361	0.11	150	628	0.25	30
40	363	0.12	150	627	0.25	30
45	371	0.13	150	627	0.25	28
50	378	0.14	150	626	0.25	28
55	380	0.15	150	626	0.25	28
60	386	0.17	150	625	0.25	25
65	385	0.18	150	630	0.25	25
70	394	0.19	150	624	0.25	25
85	394	0.23	150	632	0.24	25
100	403	0.26	150	633	0.25	25
120	411	0.30	150	632	0.25	25
150	425	0.36	150	632	0.25	25

Tab. 1. The detailed deposition parameters of the TiC/a:C thin films.

The crystalline structure of the films was determined by High Resolution Transmission Electron Microscopy (HRTEM, JEOL 3010) with an accelerate voltage of 300 kV. The thin films were thinned cross sectionally to the HRTEM investigations with ion beam milling. Fast Fourier Transform (FFT) algorithm and Selected Area Electron Diffraction (SAED) were used for the phase analysis.

Near-infrared Raman Spectroscopy (NIRS) a powerful and label-free vibrational spectroscopy technology in structure analysis was used to characterize the amorphous part of the TiC/a:C thin film through its bonding configuration. The measurements have been carried out with a Renishaw1000 B micro-Raman spectrometer using a 488 nm line of an Ar-ion laser as excitation source.

The X-ray Photoelectron Spectroscopy (XPS) is a surface-sensitive quantitative spectroscopic technique whereupon the elemental composition of the TiC/a:C based thin films was measured by this method using Al anode. 5 x 5 mm sized specimens were cut out and introduced to the chamber for analysis. The oxide layer was removed from the film surface by Ar ion sputtering in order to detect the internal composition of the films. Glancing angle (80° angle of incidence) ion beam and low ion energy (1 keV) were used to limit the possible damage of the top surface of the films. The XPS spectra were acquired using special CMA with retarding field (type DESA 105 made by Staib Instruments Ltd). Constant 1.5 eV energy resolution was applied for all measurements. Composition was determined from the main XPS lines of the constituents as follows: C - 1s at 284.4 eV, Ti - 2p ½ + $^{3}/_{2}$ at 454.0 eV, O - 1s at 530.0 eV and Ar - 2p at 242 eV. The line intensities were calculated from peak areas using Gaussian/Lorentzian peak fitting after a Shirley-background subtraction. The peak fitting made possible the decomposition of carbon line for carbide part and amorphous C part (because of their different binding energies) applying separate component peaks. The composition was determined using sensitivity factors from [17]. The background pressure was 1 x 10^{-9} mbar that was increased up to 2 x 10^{-7} mbar during Ar ion bombardment. While the original surface was stable during the measurement, the sputtered surface was found to be active, slowly accumulating graphite type carbon from the vacuum environment. In case of those specimen containing small amount of amorphous C beside of huge carbide peak, a longer data acquisition time (2 - 4 hours) was applied for accurate measurement. Special attention was given for the proper sputtering conditions to avoid the surface contamination.

3. Results

Detailed HRTEM observations about the growing of TiC/a:C thin films are shown in *Fig. 1*. The schematic zone diagram (SZD) of the two-component system [18] (*Fig. 3)* may be useful for the characterization of the growth of deposited TiC/a:C thin films. The HRTEM

investigations and FFT confirm the amorphous phase without any TiC crystals in the case of samples deposited at 5 - 10 W of Ti target power *(Fig. 1a, b)* as illustrated in the first part of SZD as well (*Fig. 3)*. The reason of the growth of individual crystals in two component system is the C segregation and repeated nucleation of the TiC nanoparticles as shown in the second part of SZD (*Fig. 3)*. Consequently, the nanocrystalline formation inside the amorphous phase was first observed at 15 - 20 W of Ti target power (*Fig. 1c, d*).

The globular TiC nanocrystals with average size of 1 - 8 nm, covered by a very thick ~ 10 nm layer of amorphous carbon, began to take shape between 25 - 35 W of Ti target power while FFT confirm the presence of the cubic TiC phase *(Fig. 1e, f, g)*. This growth is characteristic for the third part of SZD *(Fig. 3)*. The nanometer-sized columnar TiC crystallites embedded in carbon matrix became increasingly observable due to the increasing titanium content in the layer. Namely, in the case of 40 - 50 W of Ti target power *(Fig. 1h, i, j)*, the films were grown by columnar crystals with 4 - 16 nm width and among them 2 - 3 nm thin amorphous matrix as it is shown in the fourth part of SZD *(Fig. 3)*. The crystalline grains along with Moiré patterns as shown in *Fig. 1j* - in the case of 50 W of Ti target power- which indicates the overlapping of TiC columnar nanocrystals. The columns are extending through the whole film between 55 - 70 W of Ti target power *(Fig. 1k, l, m, n)*. In these films, approximately 8 - 26 nm width and fully length columns are separetad by 1 - 2 nm thin carbon matrix. This is illustrated in the last part of the SZD (*Fig. 3*). In all cases, the present crystalline phase was identified by FFT as a face-centered-cubic (fcc) TiC. The structural study performed by cross-sectional HRTEM imaging showed the increasing tendence of TiC crystals with increasing of the Ti content in the films (*Fig. 1a-n*). The same experiences were shown by *Martínez et al.* [14], namely, the samples with a lower amount of a:C has basically a polycrystalline nature and the elongated shape of the TiC crystallites can be explained by considering the columnar growth of these coatings [18]. These observations also showed a

good agreement with the work of *El Mel et al*. [19]. Furthermore, *Grigore et al.* [20] demonstrated that the increased crystallite size resulted in increased microstress in the films.

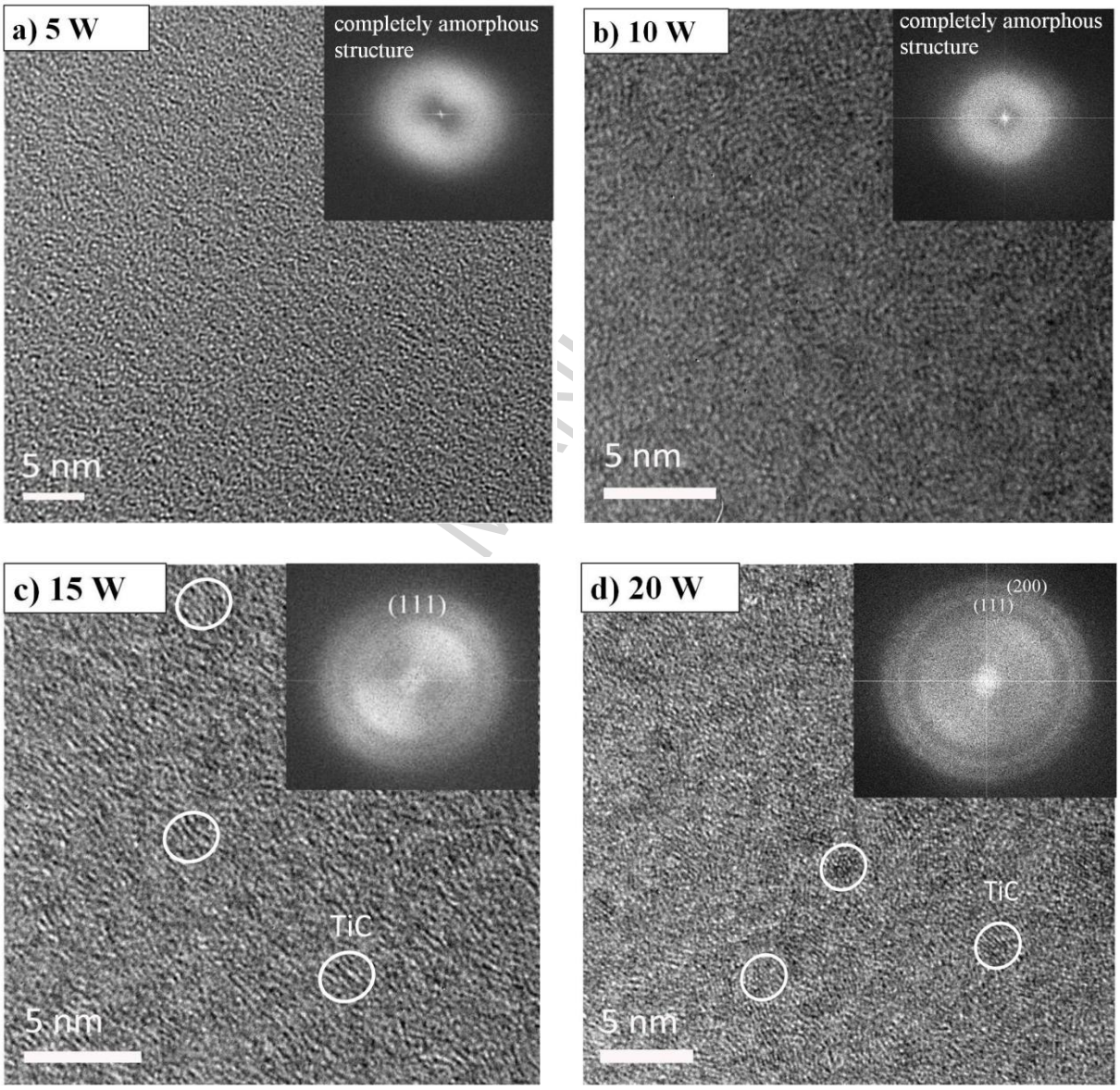

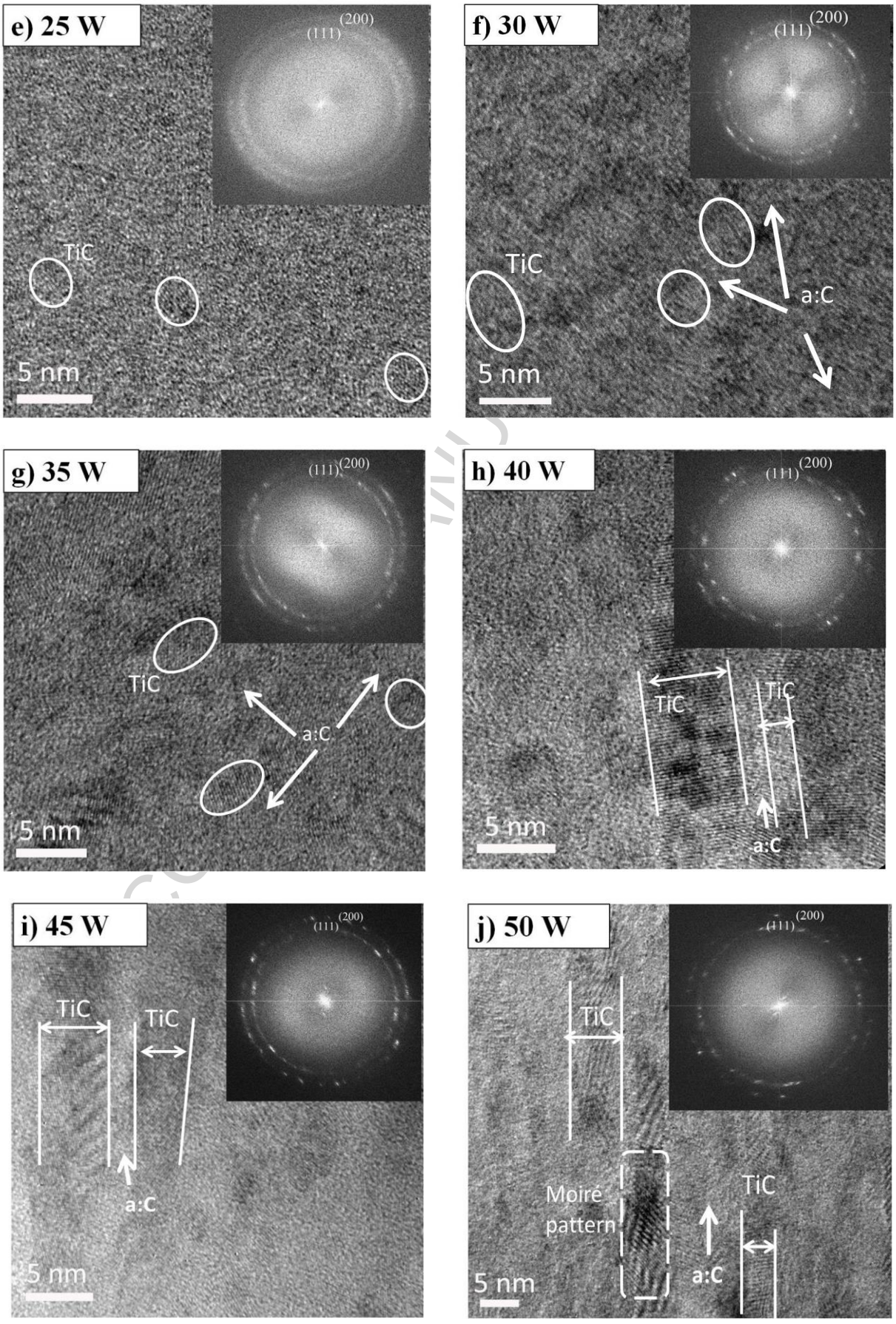
e) 25 W
(111)
(200)
TiC
5 nm
f) 30 W
(111)
(200)
TiC
a:C
5 nm
g) 35 W
(111)
(200)
TiC
a:C
5 nm
h) 40 W
(111)
(200)
TiC
TiC
a:C
5 nm
i) 45 W
(111)
(200)
TiC
TiC
a:C
5 nm
j) 50 W
(111)
(200)
TiC
Moiré pattern
TiC
a:C
5 nm

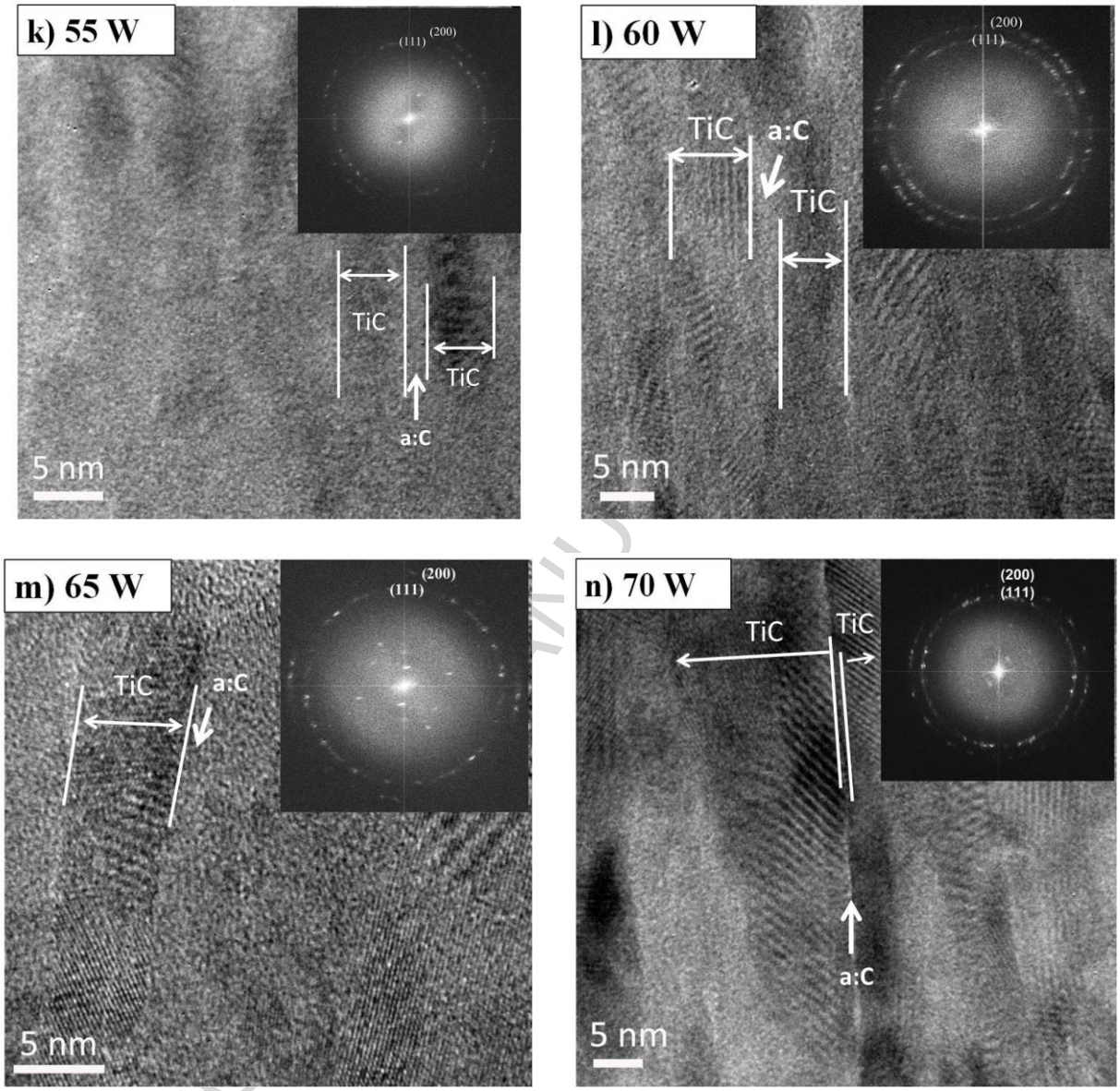

Fig. 1. Structural investigation of TiC/a:C films by HRTEM deposited at various power of Ti target and FFT for the whole images.

The further increasing of P_{Ti} from 70 W to 150 W showed the fully length TiC columns with fcc phase (*Fig. 2*). In the case of this coatings contain higher Ti concentration, the typical 002 diffuse line for amourphous carbon was not observed as the *Fig. 2* represents. On the other hand, any other Ti phase, such as hcp Ti, was not demonstrated. The last part of the SZD illustrates this type of film´s growth (*Fig. 3*).

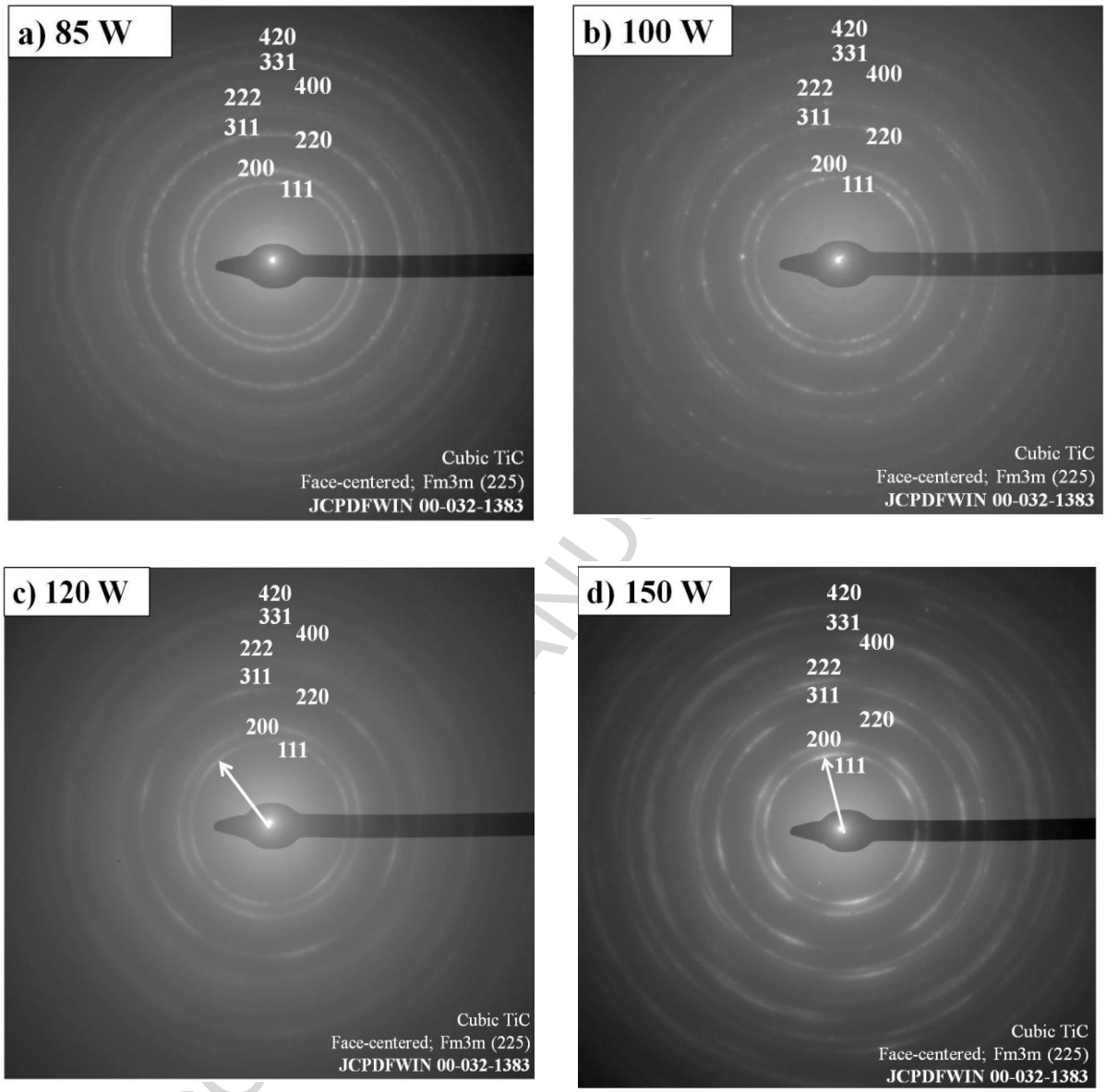

Fig. 2. SAED of TiC/a:C thin films deposited at the highest values of P_{Ti}.

According to the model of Thornton concerning the coating morphologies, the columnar structure is characteristic for films deposited at low substrate temperature and this type of structure becomes more distinct with the increase of Ti content [20].

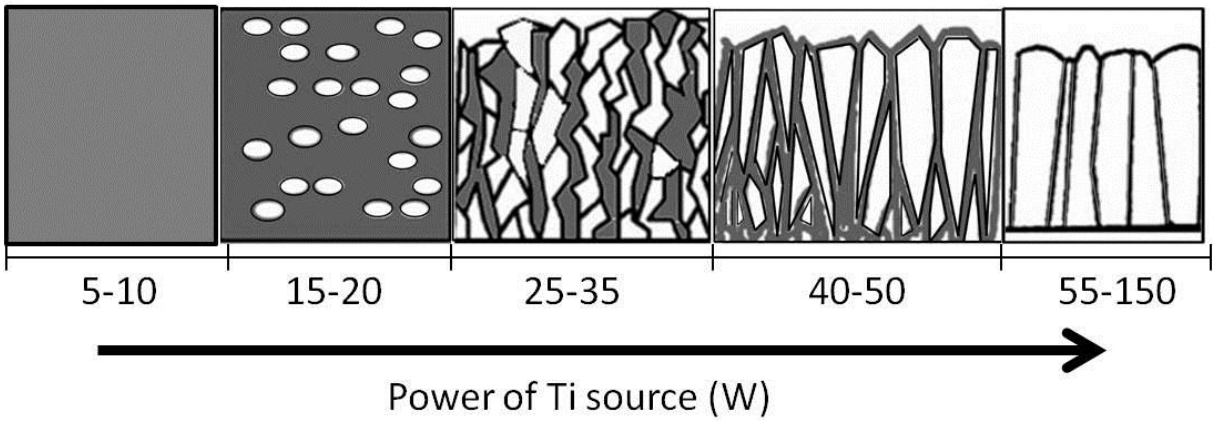

Fig. 3. The SZD of two-component system as a function of the incident first component to second component fraction volume (white - TiC particles/columns, grey- amorphous carbon).

Estimated data for the coating thickness, diameter and thickness of the TiC nanocrystallites are shown in the *Tab. 2*. These data are calculated according to the cross-sectional TEM images and also illustrate the changes which take place in the structure of the films at different compositions depending on the Ti target power.

P_{Ti} (W)	P_C (W)	t (min)	Coating thickness (nm)	Diameter of TiC particles (nm)	Thickness of TiC columns (nm)	Carbide/Ti ratio
5	150	30	102 ±11	0	-	0.31 ± 0.05
10	150	30	105 ± 2	0	-	0.82 ± 0.06
15	150	30	96 ± 2	0.5 - 1	-	0.39 ± 0.06
20	150	30	121 ± 5	~1	-	0.73 ± 0.06
25	150	30	135 ± 6	-	1 - 2	0.93 ± 0.06
30	150	30	113 ± 4	-	2 – 6	0.96 ± 0.08
35	150	30	153 ± 6	-	4 – 8	1.01 ± 0.08
40	150	30	137 ± 5	-	4 - 10	1.05 ± 0.08
45	150	28	144 ± 2	-	6 - 17	1.10 ± 0.08
50	150	28	158 ± 7	-	9 - 16	0.98 ± 0.09
55	150	28	146 ± 2	-	14 - 19	1.09 ± 0.09
60	150	25	152 ± 5	-	10 - 21	1.17 ± 0.09
65	150	25	169 ± 2	-	10 - 23	1.12 ± 0.10
70	150	25	180 ± 12	-	10 - 26	1.07 ± 0.10
85	150	25	200 ± 3	-	*	0.89 ± 0.05
100	150	25	200 ± 20	-	*	0.76 ± 0.05
120	150	25	280 ± 25	-	*	0.68 ± 0.05
150	150	25	331 ± 3	-	*	0.64 ± 0.05

Tab. 2. Estimated data from the cross-sectional TEM images for the coating thickness, diameter and thickness of the TiC nanocrystallite as function of Ti power and sputtering time. *Not detectable

XPS analysis was carried out on all films in order to reveal their composition. Both, elemental composition and types of chemical bonds were studied. Especially, the chemical state of carbon and Ti was determined. Some Ti-oxide was found at film surface due to the air exposure. The internal behaviour of films was measured after removing this oxide layer by ion bombardment. The detected carbon signal was decomposed for carbide and elemental

carbon parts which belongs to TiC and amorphous C phases, respectively. The XPS signal was collected from a macroscopic 5 x 5 mm area. The measured composition is an average over depth determined by the inelastic mean free paths of electrons (2.5 nm). The correlation between the carbide fraction, amorphous part of C and Ti concentration of the layers is shown in *Fig. 4.* The increasing tendency of Ti content with the increase of the Ti target power has been observed. Even the layers of the ~ 47 at% (70 W of P_{Ti}) Ti content have not enough Ti to bind the whole carbon volume, leading to a two - phase heterogeneous (TiC/a:C) system, confirmed by the shape analysis of carbon 1s signal. The XPS signal of carbon was decomposed for carbon and carbide according to their binding energy; 284.0 eV and 281.8 eV for carbon and carbide (TiC), respectively. This difference of binding energies (2.2 eV) was sufficient to carry out a reasonable decomposition of the detected combined peak. In comparison, *Raman et al.* [2] prepared non-stoichiometric thin films of Ti-C by a combination of pulsed DC (for Ti target) and normal DC (for graphite target) magnetron co-sputtering on oxidized silicon and fused quartz substrates. In that work, the C content increased to 62.5 at%, 34 at% of TiC and remaining amorphous C phases were observed, whereupon a smaller size grains were formed (this higher amount of carbon isolates the TiC crystallites and hinders their growth) which is in correlation with our measurement between 5 W and 70 W of P_{Ti} *(Fig. 4).* The formation of amorphous carbon cannot be excluded above 70 W of P_{Ti}, but its level is below the sensitivity of the XPS method.

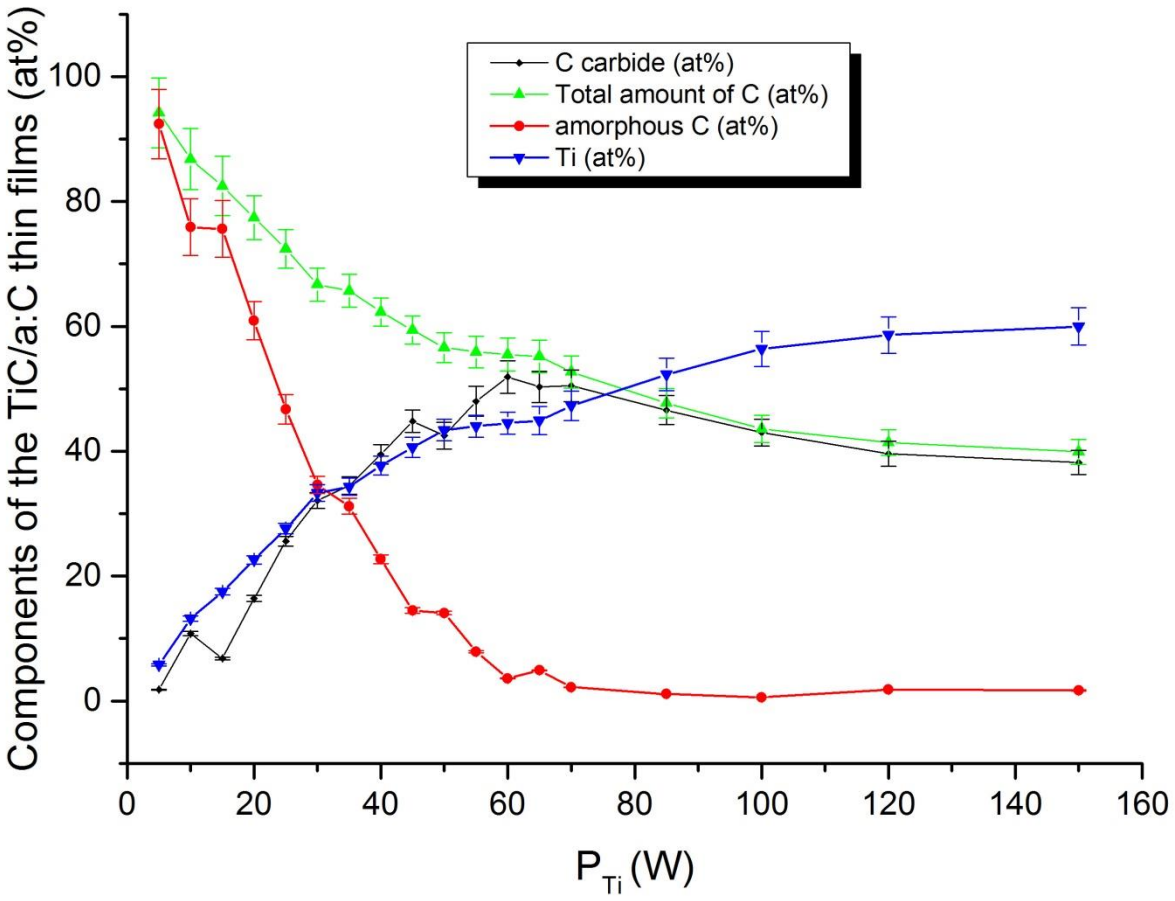

Fig. 4. Concentration of components in the TiC/a:C thin films depending on the different Ti target power as determined from XPS peaks.

The Raman spectra of the TiC/a:C thin films are shown in *Fig. 5*. The spectra were measured in the 200 - 2000 cm^{-1} wavenumber range with 488 nm excitation. A broad band of amorphous carbon was observed between 1000 and 1600 cm^{-1} for the thin film prepared with minimum Ti target power (5 W), that can be decomposed into the so called amorphous carbon D (centered around 1350 cm^{-1}) and G (around 1560 cm^{-1}) peaks. In general the two bands can be assigned to breathing vibrations of sp^2 carbon rings and stretching vibrations of sp^2 carbon rings and chains, respectively. Separation of the broad amorphous carbon peak can be observed for the sample prepared at 25 W Ti power, and low intensity broad bands appeared between 200-450 and 500-750 cm^{-1}, as well as at approximately 1000 cm^{-1}. These indicate the appearance of a disordered TiC phase. Similar results were reported in the literature by *Kumar*

et al. [21], where low deposition power (25 W) TiC peaks were centered at 221, 321, 527 and 706 cm^{-1} and these vibrational modes were found to be indicative of hypo-stoichiometric titanium carbide. The separation of the amorphous carbon peaks is even more significant at 30 W of Ti target power. A narrow band can be distinguished at 1570 cm^{-1}, overlapping the previously described G peak of amorphous carbon. Since the broader peak is also present around 1560 cm^{-1}, it can be concluded that the carbon in the sample consists of two components - one is a highly disordered carbon structure, and the other one is more ordered and (based on its position being at higher wavenumbers compared to the other one) contains higher amount of sp^2 rings (graphitic amorphous carbon). The TiC bands here became more intensive, but still broad. Based on the signal / noise ratio of 5, 25 and 30 W samples it can be concluded that the scattering contribution of the amorphous carbon became smaller. This can be due to either the decreasing amount of amorphous carbon or the increasing amount of sp^3 hybridized carbon atoms in the structure.

The Raman spectra for a:C layers produced by magnetron sputtering suggest that this type of films contains remarkable amount of graphite-like sp^2 cbonds, odd membered rings, curved graphitic sheets, and also sp^3 hibridized carbon atoms, forming diamond-like carbon structure with structural disorder of atomic bond angles and bond lengths [22]. The catalytic effect of different transition metals can result in transformation of diamond-like sp^3 carbon structure into graphite-like carbon having higher sp^2 content [23].

In case of the sample prepared at 55 W of Ti target power, a significant decrease of the peak intensity of amorphous carbon was detected, especially for the peaks belonging to the more disordered structure. The previously observed second G band still present but it is shifted towards larger wavenumbers (1590 cm^{-1}), indicating the higher level of graphitization of the structure. The TiC bands were begun to separate. Overall, the volume of the amorphous carbon matrix decreased with increasing Ti target power, whilst a more ordered and graphitic carbon structure appeared. This amorphous carbon phase was the only identifiable carbon

phase next to the TiC which was also proven by the HRTEM images. In case of the sample prepared at 70 W of Ti target power, the spectrum is dominated only by the peaks of TiC.

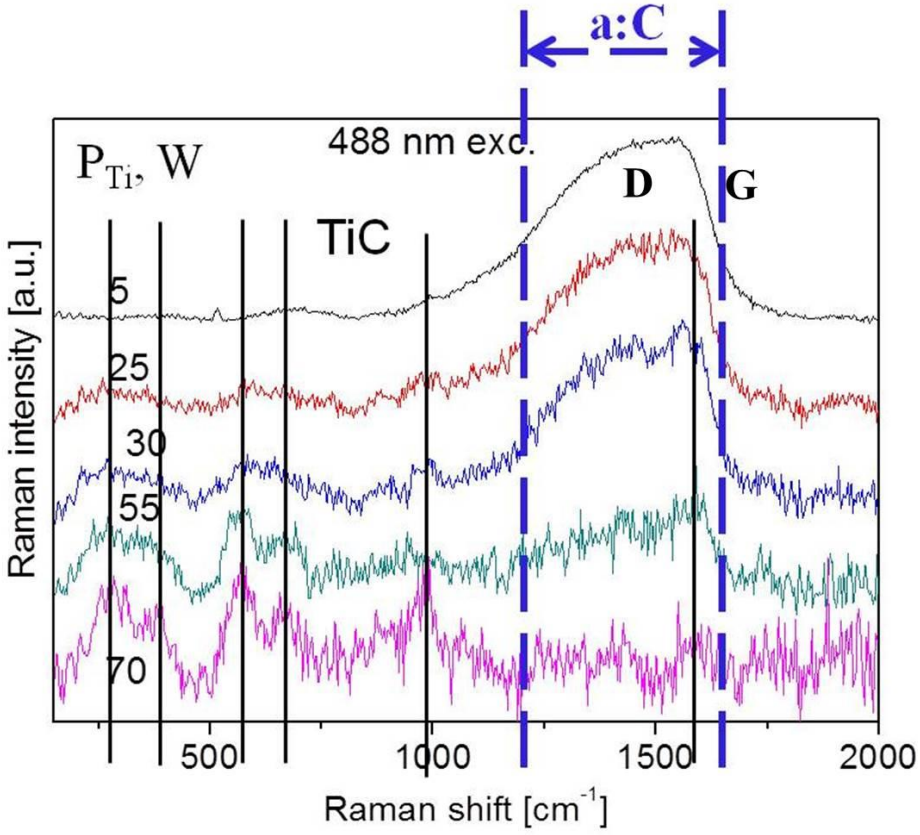

Fig. 5. Raman spectra of thin films prepared at various Ti target power (5, 25, 30, 55, 70 W) and composed of TiC nanocrystals (lines) and amorphous C (a:C with D and G lines).

4. Discussion

Titanium was deposited using a pure Ti target at the power of 100 W at four different deposition times. The thickness of the Ti layer was measured and it is shown in *Fig. 6a*. The same is shown for pure carbon in *Fig. 6b*. The last data point in *Fig. 6b* is obtained at an enlarged power of 150 W, and the resulting thickness (around 300 nm) is reduced by the coefficient of 1.5 to make it comparable with other data points of the same figure. One can see that in this way the 4 data points (and the 5th 0;0 data point) of *Fig. 6b* appear along the same straight line. This indicates that the deposited thickness of the layer is proportional to the

sputtering power, as expected. As follows from *Fig. 6a-b*, the deposited thickness is also proportional to the deposition time. The findings of *Fig. 6a-b* are summarized by the following equations:

$$d_{Ti}^{id} = k_{Ti} \cdot P_{Ti} \cdot t_{Ti} \quad (1a)$$

$$d_{C}^{id} = k_{C} \cdot P_{C} \cdot t_{C} \quad (1b)$$

where d_{Ti}^{id} (nm) and d_{C}^{id} (nm) are the deposited thicknesses of pure Ti and pure C, respectively in ideal case (when the two components do not disturb the deposition of each other), P_{Ti} (W) and P_C (W) are the sputtering powers of the Ti target and that of the C target, respectively, t_{Ti} (s) and t_C (s) are the deposition times for Ti and C, respectively, k_{Ti} (nm/J) and k_C (nm/J) are the deposition coefficients for Ti and C, respectively, in an ideal case. The latter coefficients are obtained from the slopes of regression equations of *Fig. 6a-b* as:

k_{Ti} = 1.60 ± 0.02 nm/kJ, k_C = 0.198 ± 0.002 nm/kJ

After long deposition times (see the last data points of *Fig. 6a-b*) the mass increase of the substrates were measured and from here (and from the measured the geometry of the deposited layer) the densities of the deposits were obtained as: ρ_{Ti} = 4.1 g/cm^3 and ρ_C = 2.0 g/cm^3. Let us note that these values somewhat differ from bulk density values [24]. It is in agreement with the usual observation that any property of a nano-phase (i.e. a phase with at least one of its dimensions below 100 nm) is size-dependent, including its density. Dividing the molar masses of these elements (47.9 g/mol for Ti and 12.0 for C) by their above given densities, the molar volumes are obtained as: V_{Ti} = 11.7 cm^3/mol, V_C = 6.0 cm^3/mol. Dividing *Eq. (1a-b)* by these molar volume values, the amount of deposited matter per unit surface area of the substrate is obtained as:

$$\frac{n_{Ti}^{id}}{A} = z_{Ti} \cdot P_{Ti} \cdot t_{Ti} \quad (2a)$$

$$\frac{n_{C}^{id}}{A} = z_{C} \cdot P_{C} \cdot t_{C} \quad (2b)$$

where n_{Ti}^{id} and n_{C}^{id} (mol) are the amounts of deposited Ti and carbon respectively in the ideal case (when the two components do not disturb the deposition of each other), A (m^2) is the

surface area of the substrate, $z_{Ti} \equiv \frac{k_{Ti}}{V_{Ti}}$ (mol/m^{2}J) and $z_C \equiv \frac{k_C}{V_C}$ (mol/m^{2}J) are the specific deposition coefficients of Ti and C, respectively. From the above values and definitions: $z_{Ti} = (1.37 \pm 0.03) \cdot 10^{-7}$ mol/m^{2}J and $z_C = (3.30 \pm 0.03) \cdot 10^{-8}$ mol/m^{2}J.

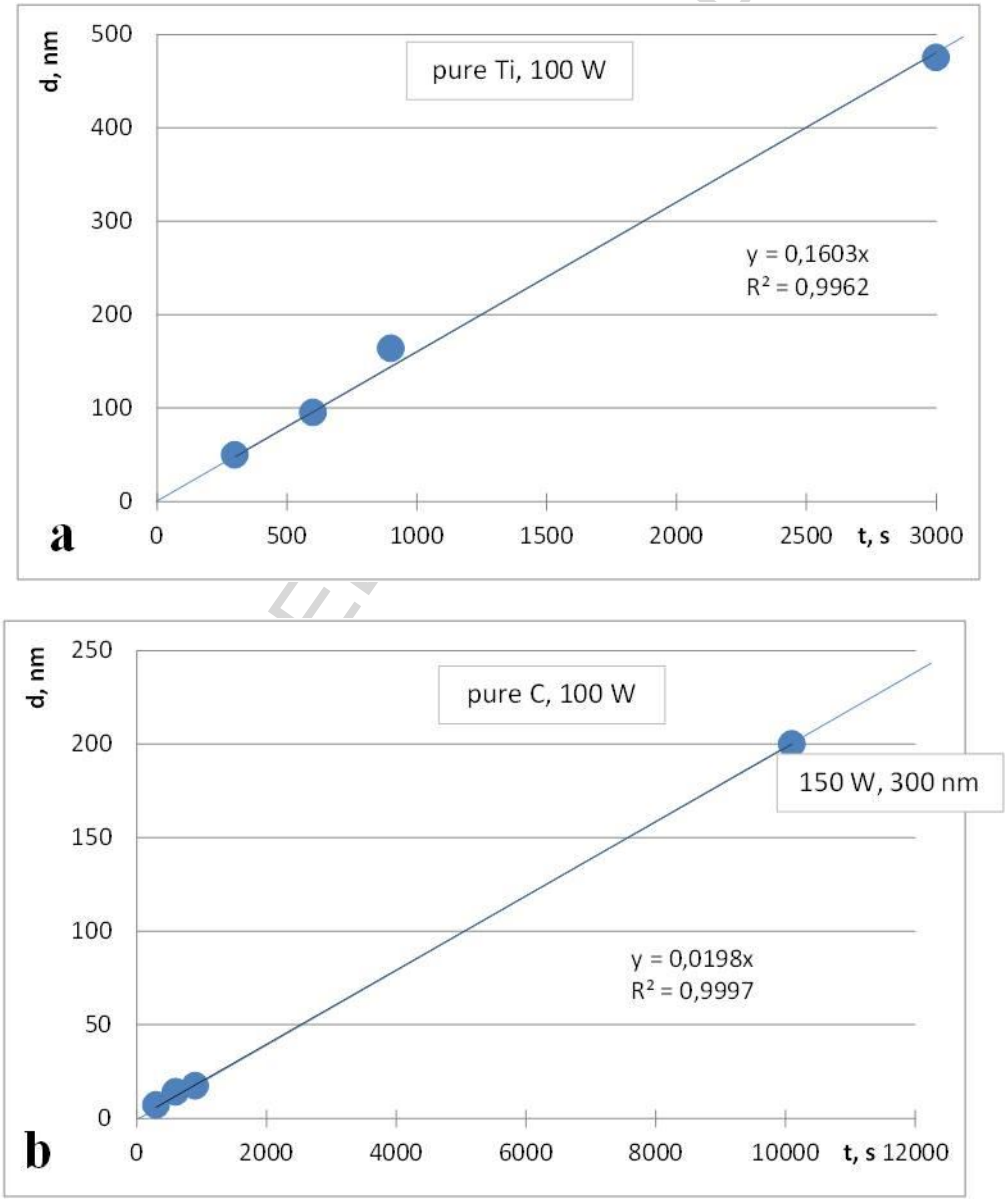

Fig. 6. The thickness of the pure Ti layer (**a**) and the pure carbon layer (**b**) as function of the deposition times at fixed sputtering power of 100 W (except the point top right in **Fig. 6b** measured at 150 W; the originally measured value (300 nm) is reduced by the coefficient of 1.5 to match it with other data points.

The Ti-C co-deposited layers where obtained using a pure Ti and a pure C targets and the same sputtering / deposition times with simultaneous sputtering / deposition of the two components on the same substrate. The sputtering power of C was selected as 150 W, while the sputtering power of Ti was gradually changed from 5 W till 150 W. In ideal case, when the two components do not influence each other during deposition, the mole fraction of Ti in the deposit can be defined as:

$$x_{Ti}^{id} \equiv \frac{n_{Ti}^{id}}{n_{Ti}^{id}+n_{C}^{id}} \tag{3a}$$

Substituting *Eq. (2a-b)* into *Eq. (3a)* at $t_{Ti} = t_C$, the following equation is obtained:

$$x_{Ti}^{id} = \frac{z_{Ti}\cdot P_{Ti}}{z_{Ti}\cdot P_{Ti}+z_C\cdot P_C} \tag{3b}$$

Substituting the above coefficients ($z_{Ti} = (1.37 \pm 0.03)\cdot 10^{-7}$ mol/m^{2}J and $z_C = (3.30 \pm 0.03)\cdot 10^{-8}$ mol/m^{2}J) and the constant value of P_C = 150 W into *Eq. (3b)*:

$$x_{Ti}^{id} = \frac{P_{Ti}}{36.1+P_{Ti}} \tag{3c}$$

where the numerical coefficient 36.1 is in W (watts).

Different measured composition values from *Fig. 4* are shown in *Fig. 7* as function of x_{Ti}^{id}, calculated by *Eq. (3c)*. As follows from *Fig. 7a*, the actually measured Ti-concentration in the deposit is significantly smaller than it follows from *Eq. (3c)*. If the linear line is drawn through the first 10 measured points in *Fig. 7a*, this line intersects the $x_{Ti}^{exp} = 0$ axes not at x_{Ti}^{id} = 0 point (as it is expected), rather at around $x_{Ti}^{id} = 0.05$. It can be explained by the following mechanism:

i. when C and Ti are sputtered simultaneously, the first deposited phase is amorphous carbon. This is because it has a much lower surface energy (0.15 J/m^2) [25] compared to the surface energy of Ti (2.57 J/m^2) [26] or TiC (2.37 J/m^2) [27]. Therefore, the energetic

barrier of nucleation of amorphous carbon is more than 1.000 times smaller than the same for Ti or TiC.

ii. Ti atoms cannot be dissolved in the amorphous carbon matrix; this is because their molar volume (atomic size) is about double than that of amorphous carbon. Although it is not a strict rule for amorphous phases, it seems to work here, as well.

iii. Ti atoms can be deposited from the gas phase in presence of amorphous carbon in the form of TiC; this nucleation process needs some super-saturation of Ti atoms in the gas phase. Titanium atoms appear not in the hcp-Ti form, mostly because the Gibbs energy of formation of the TiC crystal from Ti and C atoms is very negative (-181 kJ/mol [28]), i.e. the TiC form of Ti is much more stable in presence of amorphous carbon, compared to the hcp-Ti form (the surface energies of Ti and TiC are similar).

The above conclusions are also in good agreement with the straight line drawn through the first 10 measured points in *Fig. 7b*; here the line intersects $x_C^{am} = 1$ (the mole fraction of amorphous carbon in the deposit) also not at $x_{Ti}^{id} = 0$ point (as expected), but also at the same $x_{Ti}^{id} = 0.05$ point, as above. According to *Eq. (3c)*, this value corresponds to P_{Ti} = 2.1 W. Thus, we can conclude that when C and Ti are sputtered together at P_C = 150 W, pure amorphous carbon with no titanium will be deposited at $P_{Ti} \leq 2.1$ W. At $P_{Ti} > 2.1$ W the nucelation of TiC phase becomes possible and the mechanical mixture of TiC particles in the amorphous carbon matrix is formed.

As follows from *Fig. 7a*, at middle x_{Ti}^{id} values the experimental points increase almost with the same slope as expected for the ideal deposit. Thus, the growth of the TiC phase within the amorphous carbon matrix is not inhibited in the range of $0.05 \leq x_{Ti}^{id} \leq 0.57$, corresponding to $2.1 \leq P_{Ti} \leq 54$ (W) at P_C = 150 W.

When the x_{Ti}^{id} value exceeds 0.57 (corresponding to P_{Ti} = 54 W at P_C = 150 W), a new kinetic barrier of further Ti deposition occurs, which is manifested in nearly no further increase in x_{Ti}^{exp} in *Fig. 7a* in the interval of $0.57 \leq x_{Ti}^{id} \leq 0.63$ (corresponding to $54 \leq$

$P_{Ti} \leq 70$ (W) at P_C = 150 W). This is because in this interval the amount of amorphous carbon would become zero, if further Ti is deposited and leads to the transformation of the remaining amorphous carbon into TiC. However, as follows from *Fig. 7b*, this does not happen: the mole fraction of amorphous carbon stabilizes at low, but positive values (*Fig. 4 and Fig. 7b*). This is probably due to the interfacial stabilization of TiC nanocrystals by the thin amorphous carbon layer, separating them. If this amorphous layer disappeares, the TiC crystals would have high-energy TiC/TiC grain boundaries. This is because the surface energy of TiC is high, and if two such growing TiC crystals meet at a common interface, they are expected to form a high-energy, high-angle grain boundary. However, if a low surface energy amorphous carbon separates the TiC crystals, the resulting interfacial energy will be much lower. Therefore, the TiC nanocrystals separated by a thin a:C layer will have a smaller total energy than the same without the thin amorphous carbon layer [29].

Another principal possibility to deposit further Ti atoms with keeping the thin amorphous layer between the TiC crystals would be the decrease of the carbon content in the TiC phase, i.e. the increase of its solubility interval. As follows from *Fig. 7c*, this is exactly what is happening starting from 70 W of Ti power. The C-content of TiC in our nano-deposit becomes much lower than follows from the macroscopic phase diagram of *Fig. 8*. It is very important to note that no hcp-Ti phase forms even when the ideal Ti-content is up-to 80 at%, and even the measured Ti-content is up-to ~ 60 at%, despite what is expected based on the macroscopic phase diagram of *Fig.8*. This means that the phase formation of Ti-C nano-layers in our process does not follow the macroscopic phase diagram. It also does not follow the ideal case written by *Eq. (3c)*; in other words, different interfacial energies of different phases (amorphous carbon, TiC, hcp-Ti) and their different nucleation barriers have a significant influence on the phase constitution and micro-structure of the nano-deposit, which cannot be predicted from the calibration curves of *Fig. 6* or from the macroscopic phase diagram of *Fig. 8.*

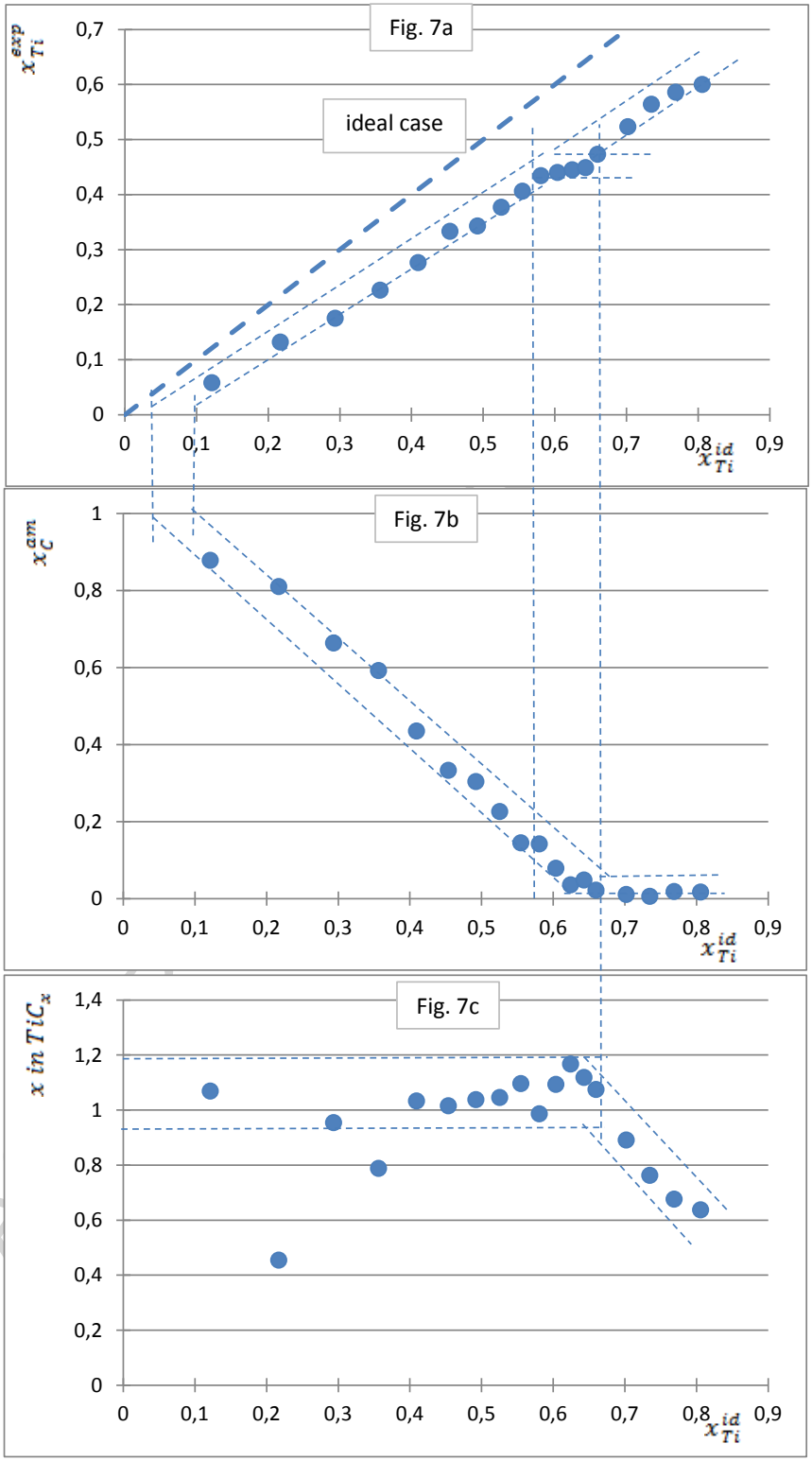

Fig. 7. The measured mole fraction of Ti in the deposited layer (***7a***), the measured mole fraction of amorphous carbon in the deposited layer (7***b***) and the measured value of x in TiC_x (***7c***) as a function of the ideal mole fraction of Ti in the deposited layer, calculated by *Eq. (3c)* (the measured values are taken from *Fig. 4*). The dashed line showed the ideal line (***7a***) and it is crossing the zero.

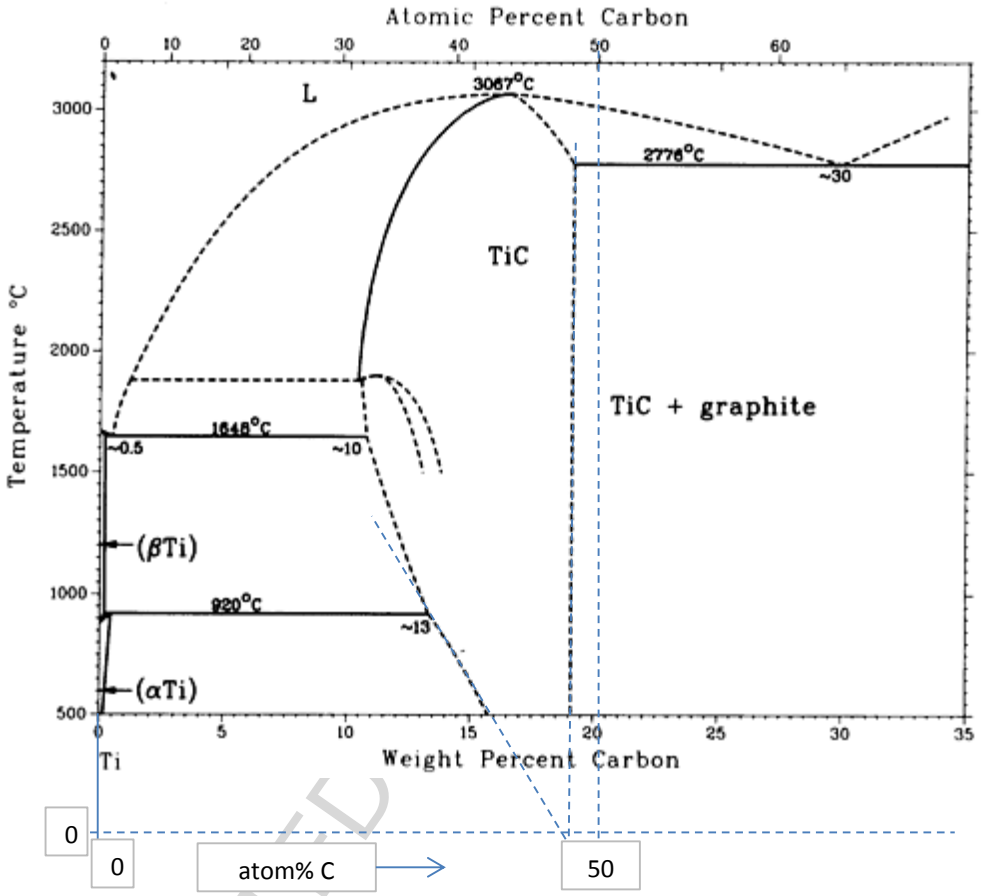

Fig. 8. The equilibrium phase diagram of the macroscopic Ti-C system [30] with extended solvus lines of the TiC phase to 0 ^{o}C.

5. Conclusion

The effect of titanium content on the growth mechanism and formation of TiC crystals in two component C-Ti films during the magnetron sputtering process was studied.

The HRTEM investigations and FFT confirm the presence of an amorphous phase in samples prepared with 5-10 W Ti target power with some ordering indicated by the XPS results. It is explained by the fact that amorphous carbon has more than 10 times lower surface energy compared to alternative phases hcp-Ti or fcc-TiC, and therefore it has more than 1.000 times less nucleation energy barrier. Ti atoms are not able to dissolve in the

amorphous carbon matrix due to their much larger atomic size. Therefore, below 2.1 W of Ti sputtering power (at 150 W of C sputtering power) almost pure amorphous carbon is formed.

Formation of fcc TiC crystals was first observed at 15 W Ti target power. Nanoparticles having globular character with average size of 1-8 nm and covered by approximately 10 nm thick amorphous carbon layer were observed in this strucutre. It is explained by the quite negative Gibbs energy of formation of TiC from elementar C and Ti. Thus, it is preferential compared to the formation of hcp-Ti in the presence of amorphous carbon (note: hcp-Ti and fcc-TiC have similar surface energies). However, the nucleation of TiC needs some oversaturation of Ti atoms in the gas phase. To ensure this, the sputtering power of Ti should be at least 2.1 W (at constant 150 W of sputtering power of C).

The structural change of TiC crystals from globular to columnar begins from 40 W Ti target power. The thickness of amorphous carbon matrix decreases from 10 nm to ~ 1 nm simultaneously with the increasing Ti content from ~ 6 at% to 60 at%. The presence of fcc TiC crystalline phase is confirmed in all cases. The evolution of the structure was clearly seen in the Raman spectra, showing the decrease of amorphous carbon content and formation of TiC structure with increasing Ti target power. Further growth of TiC crystals take place without further kinetic limitations. When the sputtering power of Ti is increased further, the growth of TiC crystals continues with increasing its Ti-content above the level, known for macro-sized TiC crystals. Interestingly, hcp-Ti does not form despite the macroscipic phase diagram.

When two or more elements are sputtered simultaneously during magnetron sputtering, the composition of the deposited layer cannot be precisely predicted from the ratio of the sputtering powers of the components alone. The composition and the structure of the nanocomposite thin films is also influenced by interfacial energies, nucleation barriers and nano-thermodynamics of different phases. Thus, the knowledge of interfacial energies of all

possible phases is needed to predict correctly the composition and morphology of different phases in the deposits obtained during magnetron sputtering.

Acknowledgements

Nikolett Oláh thanks to Young Research Fellowship of Hungarian Academy of Sciences (FIKU).

References

[1] K. Sedláčková, P. Lobotka, I. Vávra, G. Radnóczi, Structural, electrical and magnetic properties of carbon-nickel composite thin films, Carbon 43 (2005) 2192-2198.

[2] K.H.T. Raman, M.S.R.N. Kiran, U. Ramamurty, G. Mohan Rao, Structure and mechanical properties of Ti-C films deposited using combination of pulsed DC and normal DC magnetron co-sputtering, Appl. Surf. Sci. 258 (2012) 8629-8635.

[3] A. Contreras, C. Angeles-Chávez, O. Flores, R. Perez, Structural, morphological and interfacial characterization of Al-Mg/TiC composites, Mater. Char. 58 (2007) 685-693.

[4] O. Verezub, Z. Kálazi, G. Buza, N.V. Verezub, G. Kaptay, In-situ synthesis of a carbide reinforced steel matrix surface nanocomposite by laser melt injection technology and subsequent heat treatment, Surf. Coat. Technol. 203 (2009) 3049-3057.

[5] A. Ignaszak, C. Song, W. Zhu, J. Zhang, A. Bauer, R. Baker, V. Neburchilov, S. Ye, S. Campbell, Titanium carbide and its core-shelled derivative TiC@TiO2 as catalyst supports for proton exchange membrane fuel cells, Electrochim. Acta 69 (2012) 397-405.

[6] Y.C. Kimmel, L. Yang, T.G. Kelly, S.A. Rykov, J.G. Chen, Theoretical prediction and experimental verification of low loading of platinum on titanium carbide as low-cost and stable electrocatalysts, J. Catal. 312 (2014) 216-220.

[7] J. Chen, W. Li, W. Jiang, Characterization of sintered TiC-SiC composites, Ceram. Int. 35 (2009) 3125-3129.

[8] J. Cabrero, F. Audubert, R. Pailler, Fabrication and characterization of sintered TiC-SiC composites, J. Eur. Ceram. Soc. 31 (2011) 313-320.

[9] M. Zhou, P.D.D. Rodrigo, X. Wang, J. Hu, S. Dong, Y.-B. Cheng, A novel approach for preparation of dense TiC-SiC nanocomposites by sol-gel infiltration and spark plasma sintering, J.Eur. Ceram. Soc. 34 (2014) 1949-1954.

[10] N. Oláh, Zs. Fogarassy, M. Furkó, Cs. Balázsi, K. Balázsi, Sputtered nanocrystalline ceramic TiC/amorphous C thin films as potential materials for medical applications, Ceram. Int. 41 (2015) 5863-5871.

[11] K. Balázsi, M. Vandrovcová, L. Bačáková, Cs. Balázsi, Structural and biocompatible characterization of TiC / a:C nanocomposite thin films, Mat. Sci. Eng. C 33 (2013) 1671-1675.

[12] K. Balázsi, I.E. Lukács, S. Gurbán, M. Menyhárd, L. Bačáková, M. Vandrovcová, C. Balázsi, Structural, mechanical and biological comparison of TiC and TiCN nanocomposites films, J. Eur. Ceram. Soc. 33 (2013) 2217-2221.

[13] N. Arshi, J. Lu, C.G. Lee, J.H. Yoon, B.H. Koo and F. Ahmed, Thickness effect on properties of titanium film deposited by d. c. magnetron sputtering and electron beam evaporation techniques, Bull. Mater. Sci. 36 (2013) 807-812.

[14] D. Martínez-Martínez, C. López-Cartes, A. Fernández, J.C. Sánchez-López: Influence of the microstrucutre on the mechanical and tribological behavior of TiC/a-C nanocomposite coatings, Thin Solid Films 517 (2009) 1662-1671.

[15] A.Z.A. Djafer, N. Saoula, N. Madaoui, A. Zerizer, Deposition and characterization of titanium carbide thin films by magnetron sputtering using Ti and TiC targets, Appl. Surf. Sci. 312 (2014) 57-62.

[16] N. Oláh, M. Veres, A. Sulyok, M. Menyhárd, J. Gubicza, K. Balázsi, Examination of nanocrystalline TiC/amorphous C deposited thin films, J. Eur. Ceram. Soc. 34 (2014) 3421-3425.

[17] Handbook of Monochromatic XPS Spectra, The elements and Native Oxides, ed. B. Vincent Chris, Wiley 2000.

[18] I. Petrov, P.B. Barna, L. Hultman, J.R. Greene, Microstructural evolution during film growth, J. Vac. Sci. Technol. A21 (2003) 117-127.

[19] A.A. El Mel, E. Gautron, F. Christien, B. Angleraud, A. Granier, P. Souček, P. Vašina, V. Buršíková, M. Takashima, N. Ohtake, H. Akasaka, T. Suzuki, P.Y. Tessier, Titanium carbide/carbon nanocomposite hard coatings: A comparative study between various chemical analysis tools, Surf. Coat. Technol. 256 (2014) 41-46.

[20] E. Grigore, C. Delacote, A.A. El Mel, M. Boujtita, A. Garnier, P.Y. Tessier, Structural characterization and electrochemical behavior of titanium carbon thin films, Surf. Coat. Technol. 211 (2012) 192-195.

[21] N. Kumar, G. Natarajan, R. Dumpala, R. Pandian, A. Bahuguna, S.K. Srivastava, T.R. Ravindran, S. Rajagopalan, S. Dash, A.K. Tyagi, M.S.R. Rao, Microstructure and phase composition dependent tribological properties of TiC/a-C nanocomposite thin films, Surf. Coat. Technol. 258 (2014) 557-565.

[22] A.A. Voevodin, M.A. Capano, S.J.P. Laube, M.S. Donley, J.S. Zabinski, Design of a Ti/TiC/DLC functionally gradient coating based on studies of structural transitions in Ti–C thin films, Thin Solid Films 298 (1997) 107-115.

[23] Q.N. Meng, M. Wen, F. Mao, N. Nedfors, U. Jansson, W.T. Zheng, Deposition and characterization of reactive magnetron sputtered zirconium carbide films, Surf. Coat. Technol. 232 (2013) 876-883.

[24] D.R. Lide, CRC Handbook of Chemistry and Physics, ed. CRC Press, 1993-94.

[25] P. Baumli, G. Kaptay, Wettability of carbon surfaces by pure molten alkali chlorides and their penetration into a porous graphite substrate, Mat. Sci. Eng. A 495 (2008) 192-196.

[26] L.Z. Mezey, J. Giber, The surface free energies of solid chemical elements: calculation from internal free enthalpies of atomization, Jpn. J. Appl. Phys. 21 (1982) 1569-1571.

[27] G. Kaptay, Modeling Interfacial Energies in Metallic Systems, Mat. Sci. Forum 473-474 (2005) 1-10.

[28] I.Barin, Thermochemical Properties of Pure Substances, VCh, 1993, in 2 parts.

[29] G. Kaptay, Nano-Calphad: extension of the Calphad method to systems with nano-phases and complexions, J. Mater. Sci. 47 (2012) 8320-8335.

[30] T.B. Massalski (ed), Binary Alloy Phase Diagrams, second ed., 3 volumes, ASM International, 1990.

Highlights

- The effect of Ti content on the growth mechanism of TiC/a:C thin films was studied.
- The thickness of a:C matrix decreases simultaneously with the increasing Ti content.
- Only the presence of fcc TiC crystalline phase was detected in all cases.
- Interfacial energies and nucleation barriers are used to explain the results.